Talanta 222 (2021) 121522

Contents lists available at ScienceDirect

Talanta

journal homepage: www.elsevier.com/locate/talanta

# Redox reaction-modulated fluorescence biosensor for ascorbic acid oxidase assay by using $MoS_2$ quantum dots as fluorescence probe

Ning Li [a,b,1], Feng Zhang [a,1], Wenying Sun [a], Lili Zhang [c], Xingguang Su [a,*]

[a] Department of Analytical Chemistry, College of Chemistry, Jilin University, Changchun, 130012, PR China
[b] Department of Respiratory, The Third Hospital of Jilin University, Changchun, 130012, China
[c] State Key Laboratory of Inorganic Synthesis & Preparative Chemistry, Jilin University, Changchun, 130012, PR China

ARTICLE INFO

*Keywords:*
$MoS_2$ quantum dots
CoOOH nanoflakes
Ascorbic acid oxidase
Ascorbic acid
Fluorescence resonance energy transfer

ABSTRACT

Herein, a sensitive fluorescence (FL) biosensor for the assay of ascorbic acid oxidase (AAO) was established based on the fluorescence resonance energy transfer (FRET) between $MoS_2$ quantum dots (MQDs) and CoOOH nanoflakes. CoOOH nanoflakes as effective FL quencher could quench the FL signal of MQDs on the basis of FRET. When ascorbic acid (AA) was added to the MQDs/CoOOH nanoflakes system, the FL signal was restored due to the redox reaction between CoOOH nanoflakes and AA, in which CoOOH nanoflakes were reduced to $Co^{2+}$ by AA. In the presence of AAO, the recovered FL signal of MQDs was quenched again because of the enzymatic catalytically reaction between AAO and AA, in which AA was oxidized to dehydroascorbic acid (DHA) and then prevented the decomposition of CoOOH nanoflakes. Under the optimal experimental conditions, this developed fluorescence method exhibited good linear ranges from 2 to 10 mU $mL^{-1}$ and 10–40 mU $mL^{-1}$ with a low detection of limit of 0.8 mU $mL^{-1}$ for AAO detection. And the limit of quantification (LOQ) of 2.6 mU $mL^{-1}$ was obtained. The proposed biosensor showed high sensitivity and selectivity, and was successfully applied for AAO determination in human serum samples.

## 1. Introduction

As a key element of nanotechnology and science, nanomaterials have gained tremendous research interests [1,2]. Recent booming developments in emerging quantum dots (QDs) with diameters often limited to 10 nm have been applied to existing and emerging nanotechnologies as a result of quantum confinement and prominent edge effects [3,4]. Among QDs, $MoS_2$ quantum dots (MQDs) which belonged to representative transition metal dichalcogenides (TMDs) nanomaterials have been widely noticed and prompted many potential applications in biosensor, bioimaging, catalysis and photodynamic therapy etc. For their fascinating optical, electrical, catalytic and biocompatibility characteristics [5–7]. Noteworthy, the excellent optical properties of MQDs enable their application as new fluorescence (FL) platforms for biosensing and bioimaging [8,9]. A variety of MQDs-based biosensing strategies have been proposed. Wang et al. [10] proposed a FL detection system for $H_2O_2$ and glucose by using MQDs as both the Fenton catalyst and fluorescence probe. And Swaminathan et al. [11] developed a turn-on FL biosensor for the detection of bovine serum albumin on the basis of Förster resonance energy transfer between MQDs and polyaniline.

Ascorbic acid oxidase (AAO) is a copper-containing enzyme that is located in the cytoplasm or binds to the cell wall [12]. AAO is coupled with other redox reactions to play the role of terminal oxidase. It can oxidize ascorbic acid (AA) to dehydroascorbic acid (DHA), thereby regulating the redox state of the ascorbic acid bank in plants apoplast, which is closely related to the growth and development of plants, and plays an important role in delaying senescence and metabolism of plants [13–15]. Moreover, AAO activities may be part of a dynamic system of plant oxygen management. Thus, the down-regulation of AAO activity has great physiological significance during fruit ripening and wound healing [16,17]. And the demands for AAO as diagnostic purpose and reagent have been increasing for vitamin C determination in foodstuffs [18]. So far, there were many analytical methods for the detection of AA, but few were used for AAO activity detection [19,20]. Wang et al. [21] reported a dual-mode strategy consisted of fluorometry and colorimetry for the assay of AA and AAO on the basis of the oxidation of *o*-phenylenediamine by permanganate. And Liu et al. [22] developed a

* Corresponding author.
*E-mail address:* suxg@jlu.edu.cn (X. Su).
[1] These authors contributed equally to this work.

https://doi.org/10.1016/j.talanta.2020.121522
Received 16 February 2020; Received in revised form 3 August 2020; Accepted 5 August 2020
Available online 9 August 2020

fluorometric and colorimetric dual-model analytical method for AA and AAO detection by AA-induced growth and aggregation of DNA-templated gold/silver nanoclusters. Thus, developing an analytical strategy for AAO activity assay with high sensitivity, selectivity and simplicity is meaningful.

CoOOH nanoflakes, as emerging 2D transition metal oxyhydroxides nanomaterials, have been applied in a variety of fields such as electrocatalysis, biocatalysis, photocarriers, supercapacitors and biosensing etc. Due to their simple and fast synthesis process, unique structure and excellent physicochemical properties [23–25]. Especially, acting as highly effective FL quencher on fluorophores makes them show great potential in biomolecular sensing owing to their high surface-to-volume ratios and good light absorption ability [26,27]. Furthermore, CoOOH nanoflakes have been utilized for AA detection by the specific redox reaction between CoOOH nanoflakes and AA [28,29]. For example, Xu et al. [30] designed a FL and photoacoustic dual-modal probe to detect AA based on CoOOH/red-emissive carbon dots nano-hybrid and the specific deoxidation of CoOOH to $Co^{2+}$ by AA. Liu et al. [31] reported a FL turn-on analysis of AA by using a hybrid material as nanoprobe which was consisted of guanine-rich single stranded DNA and CoOOH nanosheets, where CoOOH nanosheets acted as recognition components for AA detection. Feng et al. [32] constructed a two-photon nanoprobe for the detection and bioimaging of AA using CoOOH nanoflakes as FL quencher and oxidant. The above mentioned analysis strategies were all for the determination of AA by using CoOOH nanoflakes, while AAO as an enzyme can catalyze the oxidation of AA, the further broadening of CoOOH nanoflakes application for AAO detection is interesting and expectable.

In this paper, a sensitive and novel FL biosensor system on the basis of fluorescence resonance energy transfer (FRET) between MQDs and CoOOH nanoflakes was designed for the assay of AAO (Scheme 1). The ultrathin CoOOH nanoflakes acted as the FL quencher can turn off the FL signal of MQDs emitted at 416 nm by 320 nm excitation via FRET. When AA was added, CoOOH nanoflakes were reduced to $Co^{2+}$ by AA, leading to the recovery of FL signal of MQDs. In the presence of AAO, AA can be catalytically oxidized to DHA by AAO, which hindered the redox reaction between AA and CoOOH nanoflakes and lead to the FL signal decreased again. Thus, AAO can be determined sensitively and accurately by monitoring the FL signal changes based on the MQDs/CoOOH nanoflakes/AA system.

## 2. Experimental section

### 2.1. Materials and instruments

The chemicals and instruments used in the study were illustrated in Electronic Supporting Information (ESI).

### 2.2. Synthesis of MQDs and CoOOH nanoflakes

MQDs were prepared by via a bottom-up hydrothermal method with ammonium molybdate and reduced glutathione as molybdenum and sulfur sources based on literature-reported procedures with minor modifications [33]. And the simple and fast synthesis of CoOOH nanoflakes was carried out according to the previous reports [34]. The detailed synthesis operation processes of MQDs and CoOOH nanoflakes were described in the ESI.

### 2.3. Fluorescence sensing of AAO

Different concentrations AAO, 60 μL of 2 mmol $L^{-1}$ AA, 20 μL of 10 mmol $L^{-1}$, pH 7.4 phosphate buffer solution (PBS) and $H_2O$ were added into calibrated test tubes with a total volume of 790 μL enzymatic reaction solutions. And then the mixture was incubated at 37 °C for 20 min. Subsequently, 50 μL of 100 mmol $L^{-1}$, pH 5.4 PBS, 60 μL of 0.5 mg $mL^{-1}$ CoOOH nanoflakes and 100 μL MQDs (1.95 mg $mL^{-1}$) were introduced the above calibrated test tubes to give final volumes of 1.0 mL. After incubating for another 35 min at ambient temperature, the PL spectral data of the prepared samples were collected with the excitation wavelength of 320 nm.

### 2.4. Real samples assay of AAO

AAO in human serum samples were measured by the standard addition method. Various concentrations of AAO were added into the serum samples, then the serum were diluted 20 times with deionized water for the preparation of the spiked samples. Then the real samples analyses of AAO were performed using the procedure in the section of **2.3** described above.

## 3. Results and discussion

### 3.1. Characterization of MQDs and CoOOH nanoflakes

The prepared MQDs were characterized by TEM, which displayed the morphology and size of MQDs. As shown in Fig. 1A, the MQDs had a good dispersion. Meanwhile, the inset of Fig. 1A showed a narrow size distribution of MQDs from 1.1 to 3.0 nm with a mean diameter of 2.08 nm. Moreover, the FT-IR spectrum of MQDs in Fig. 1B displayed the possible functional groups. It can be observed that the absorption bands at 3242 $cm^{-1}$, 2164 $cm^{-1}$, 1670 $cm^{-1}$, 1406 $cm^{-1}$ and 1239 $cm^{-1}$ were belonged to the stretching vibration of the N–H, S–H, C═O, C–N and

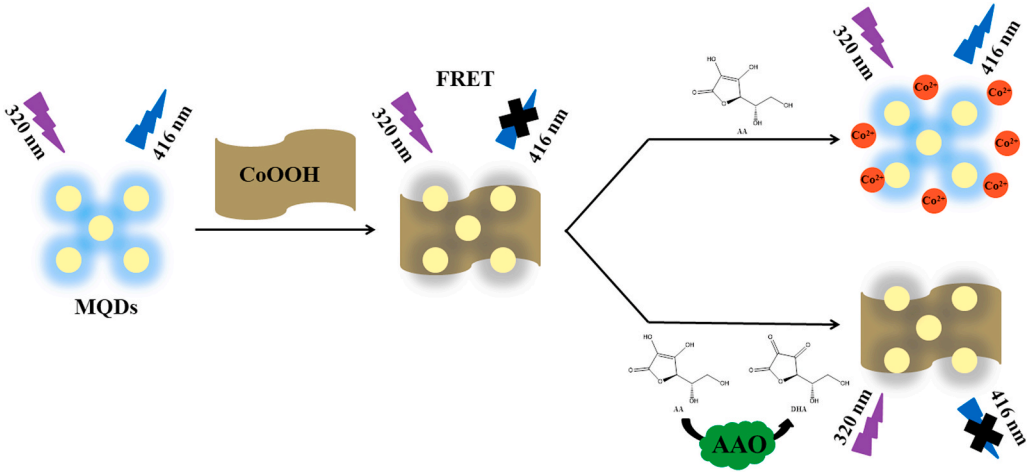


**Scheme 1.** Schematic presentation of the designed FL biosensor for AAO assay based on FRET between MQDs and CoOOH nanoflakes.

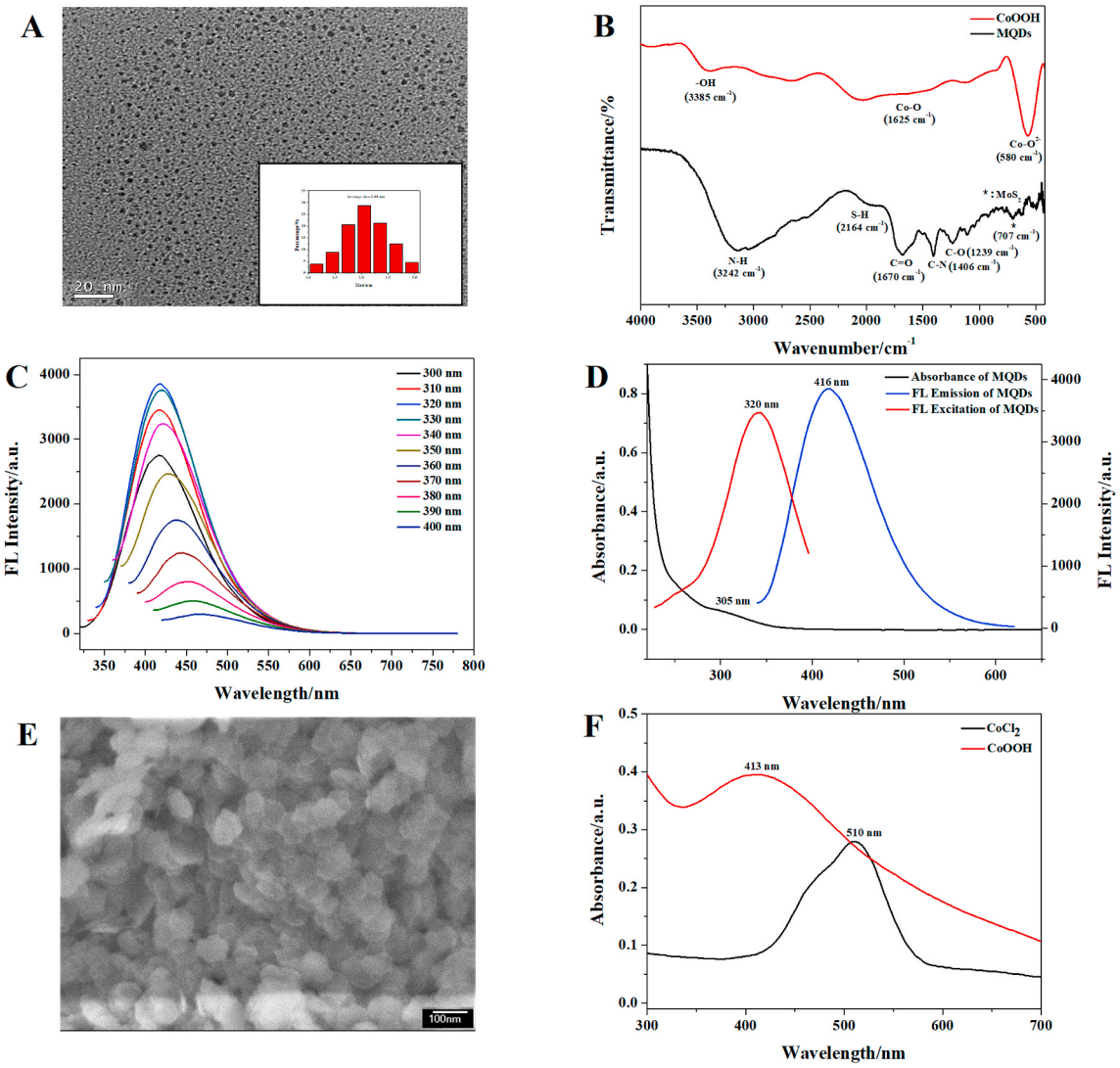


**Fig. 1.** (A) TEM image of MQDs. Inset: Diameter distribution of MQDs. (B) FT-IR spectra of CoOOH nanoflakes and MQDs. (C) FL emission spectra of MQDs excited by various wavelengths. (D) FL excitation and emission spectra of MQDs and UV–vis absorption spectrum of MQDs. (E) SEM image of CoOOH nanoflakes. (F) UV–vis absorption spectra of $CoCl_2$ and CoOOH nanoflakes.

C–O bonds, respectively [35,36]. And the peak labeled with asterisk at 707 $cm^{-1}$ was corresponded to the fingerprint characteristic absorption peak of $MoS_2$ [37]. The results from FTIR characterization revealed that there were amino, carboxylic and sulfhydryl groups likely located on MQDs surface. It can be observed from Fig. 1C, the blue-emitting MQDs showed the excitation-dependent FL properties. The FL emission wavelength showed a gradually red-shift with the excitation wavelength increasing, which can be ascribed to the different edge sites and surface defects [38]. Furthermore, the UV–vis absorption spectrum in Fig. 1D showed the excitonic absorption peak of MQDs at 305 nm which was consistent with those literature-reported previously [37]. The maximum FL emission and excitation peaks of MQDs were located at 416 nm and 320 nm, respectively (Fig. 1D).

The FT-IR spectrum of CoOOH nanoflakes was shown in Fig. 1B, it can be seen that the characteristic peak centered at 3385 $cm^{-1}$ was attributed to the hydrogen-bonded hydroxyl group (-OH) stretching vibration. And the other two characteristic absorption peaks at 1625 $cm^{-1}$ for the Co═O double bond and that at 580 $cm^{-1}$ for the Co–$O^{2-}$ bond were noticed [39]. The SEM image of CoOOH nanoflakes in Fig. 1E indicated the CoOOH nanoflakes showed the typical hexagonal nanoflakes morphology. In addition, Fig. 1F revealed the UV–vis absorption bands of $CoCl_2$ at 510 nm and the CoOOH nanoflakes at 413 nm, which had a distinct difference between the two peaks. The above results identified the successful formation of CoOOH nanoflakes.

### 3.2. *Sensing mechanism and feasibility of AAO*

As displayed in Scheme 1, the existence of CoOOH nanoflakes can cause the FL quenching of MQDs. However, the addition of AA can result in the decomposition of CoOOH nanoflakes owing to the redox reaction between CoOOH nanoflakes and AA, in which CoOOH nanoflakes was reduced to $Co^{2+}$ by AA and the quenched FL was restored simultaneously. In the presence of AAO, AA can be catalytically oxidized by AAO to DHA [15] and thence prevented the reduction of CoOOH nanoflakes by AA, thereby leading to the FL quenching again. The FL quenching mechanism of MQDs by CoOOH nanoflakes was further investigated. It can be observed from Fig. 2A, there was a relative large overlap between the UV–Vis absorbance spectrum of CoOOH nanoflakes and the FL emission spectrum of MQDs. This indicated that FRET may occur between MQDs and CoOOH nanoflakes, which MQDs served as energy donor and CoOOH nanoflakes was as acceptor, and the FRET theory was used to prove the quenching process [40,41]. According to the FL quenching of MQDs by CoOOH nanoflakes in Fig. 2B, the energy transfer efficiency (E) was calculated. The equation of $E = 1-I/I_0$ was

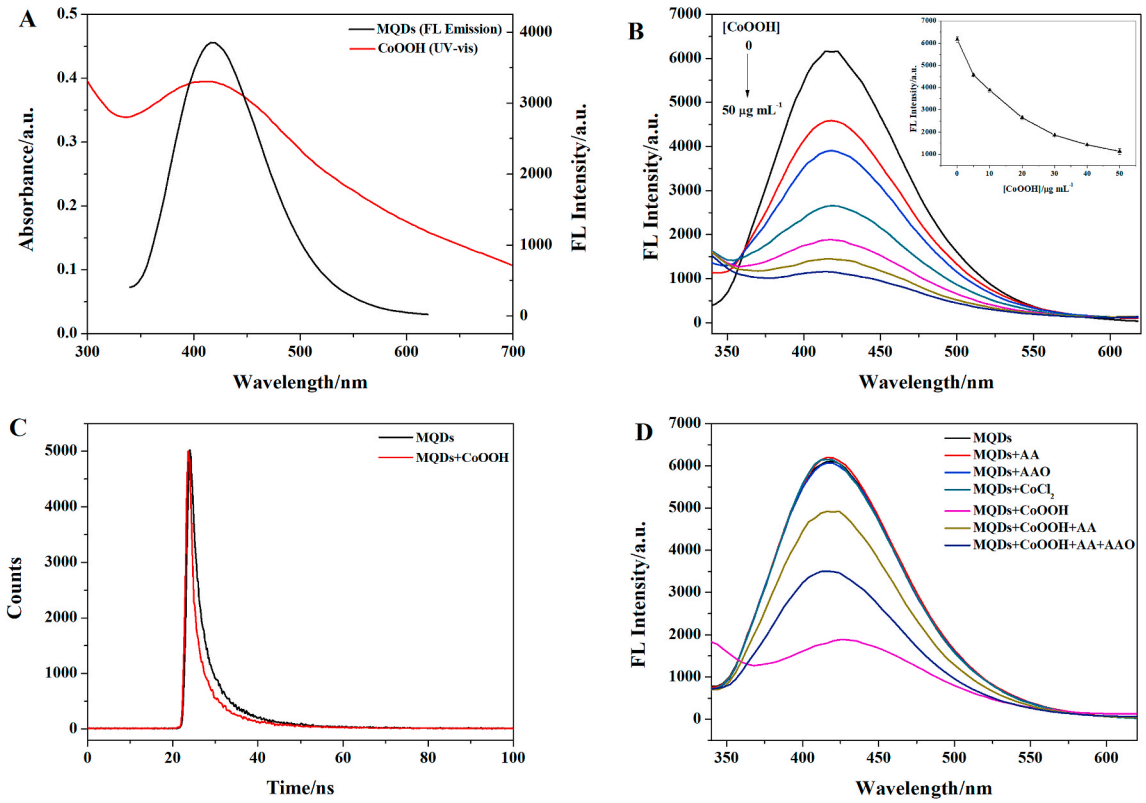


**Fig. 2.** (A) FL emission spectrum of MQDs and UV–vis absorption spectrum of CoOOH nanoflakes. (B) FL emission spectra of MQDs with various concentrations of CoOOH nanoflakes (0, 5, 10, 20, 30, 40, 50 μg $mL^{-1}$). Inset: FL intensity of MQDs with increasing CoOOH nanoflakes concentrations. (C) FL lifetime of MQDs with and without CoOOH nanoflakes. (D) FL emission spectra of MQDs, MQDs + AA, MQDs + AAO, MQDs + $CoCl_2$, MQDs + CoOOH nanoflakes, MQDs + CoOOH nanoflakes + AA and MQDs + CoOOH nanoflakes + AA + AAO system, respectively.

used in the calculation of E, where I and $I_0$ stand for the FL intensity of the donor in the presence and absence of acceptor, respectively. As shown in Fig. S1, the E increased with the increasing concentration of CoOOH nanoflakes from 5 to 50 μg $mL^{-1}$. The maximum E of 81.6% was obtained when CoOOH nanoflakes concentration was 50 μg $mL^{-1}$, and the donor-acceptor distance (R) was calculated to be 1.49 nm when E was 81.6% (the detail calculation was shown in ESI). Meanwhile, the zeta potential of MQDs and CoOOH nanoflakes were measured. As shown in Fig. S2, the CoOOH nanoflakes with positive zeta potential (14.96 mV) and MQDs with negative zeta potential (−12.71 mV) were obtained, indicating that there was electrostatic interaction between CoOOH nanoflakes and MQDs which shortened the distance between the donor and the acceptor. Consistent with the above FRET calculations, the donor-acceptor distance was less than 10 nm. Thus, the FRET effect occurred between MQDs and CoOOH nanoflakes.

Moreover, the FL lifetimes of MQDs with and without CoOOH nanoflakes were measured. As depicted in Fig. 2C, the FL lifetime of MQDs obviously decreased when the CoOOH nanoflakes were added. And the average fluorescence lifetime of MQDs in the absence ($\tau_0$) and presence ($\tau$) of CoOOH nanoflakes were $\tau_0 = 6.16$ ns and $\tau = 5.31$ ns, respectively. Meanwhile, the dynamic quenching effect (DQE) can be theoretically described by the Stern−Volmer equation: $I_0/I = 1 + Ksv[Q]$. It presents the relationship between the relative FL intensity ($I_0/I$) and the quencher concentration [Q], where I and $I_0$ represent the FL intensity in the presence and absence of quencher and Ksv stands for the Stern-Volmer quenching constant. According to the FL quenching phenomenon of MQDs in the presence of various concentrations of CoOOH nanoflakes (Fig. 2B), the linear Stern−Volmer equation with Ksv = 0.081 was obtained and displayed in Fig. S3. The above results indicated that the dynamic quenching mechanism led to the FL quenching of MQDs.

In order to verify if this designed strategy can be applied for AAO sensing, the feasibility experiments were carried out. As presented in Fig. 2D, the FL intensity of MQDs had little changes with the addition of AA, AAO and $CoCl_2$, respectively. However, the addition of CoOOH nanoflakes caused an obvious decrease in the FL intensity of MQDs. Fig. 2B displayed the FL emission spectra of MQDs with various concentrations of CoOOH nanoflakes. It can be seen from the inset of Fig. 2B that the FL intensity of MQDs decreased with the increasing concentrations of CoOOH nanoflakes. In order to obtain higher sensitivity for AAO sensing, 30 μg $mL^{-1}$ CoOOH nanoflakes was chosen in the following experiments. It can also be observed from Fig. 2D that the quenched FL of MQDs was restored when CoOOH nanoflakes and AA coexisted. Subsequently, the addition of AAO to the MQDs/CoOOH nanoflakes/AA system caused the FL intensity to decrease again owing to the enzymatic reaction between AAO and AA. These results verified the feasibility of the proposed strategy for AAO sensing.

### 3.3. *Optimization of conditions*

In this study, the experimental parameters were optimized to get better analytical performance for AAO detection. For the MQDs/CoOOH nanoflakes system and the MQDs/CoOOH nanoflakes/AA system, the effects of reaction time and pH on the FL intensity of the both systems were studied. As displayed in Fig. S4A, the FL intensity of the MQDs/CoOOH nanoflakes system can reach stable within 30 s, suggesting that the FL quenching of MQDs by CoOOH nanosheets was a fairly rapid process. Fig. S4B indicated the FL intensity of the MQDs/CoOOH nanoflakes/AA system increased with the time increasing, and kept constant until 35 min, indicating the redox reaction was completed between AA and CoOOH nanoflakes. Thus, 35 min was selected for the reaction system of MQDs/CoOOH nanoflakes/AA. Fig. S4C showed that

pH had little influence on the FL intensity of MQDs and MQDs/CoOOH nanoflakes system in the range of pH 5.0–9.0. The FL intensity of MQDs/CoOOH nanoflakes/AA system rapidly decreased in the pH range of 5.4–6.8 and then reached a balance in pH range of 7.0–9.0. The redox reaction equation between AA and CoOOH nanoflakes was as follows [29]: (1).

And acidic condition was beneficial to this reaction according to Eq. (1). Simultaneously, considering the FL quenching effect of CoOOH nanoflakes on MQDs, the FL intensity differences (ΔF) between MQDs/CoOOH nanoflakes/AA and MQDs/CoOOH system under various pH values were investigated. As shown in Fig. S4D, it can be seen that ΔF reached maximum at pH 5.4. Thus, pH of 5.4 was adopted to get the superior FL quenching and recovery. Furthermore, the FL intensity changes of the MQDs/CoOOH nanoflakes system with different AA concentrations were investigated under the optimized experimental conditions. As shown in Fig. 3A, the FL intensity of MQDs/CoOOH nanoflakes system gradually increased with the increasing concentrations of AA from 0 to 120 μmol $L^{-1}$ and the FL signals were almost constant when AA concentration increased to above 120 μmol $L^{-1}$. Correspondingly, Fig. 3B showed that a good linear relationship was obtained between the relative FL intensity ($I/I_0$) and AA concentrations in the range of 10–120 μmol $L^{-1}$ with a linear regression equation of $I/I_0 = 0.0095$ [AA] + 0.976 ($R^2 = 0.987$). And 120 μmol $L^{-1}$ AA was used in the following experiments for AAO detection.

The effect of enzymatic reaction pH, temperature and time between AAO and AA were investigated. The influence of pH and temperature were illustrated in Fig. S5A and Fig. S5B, it can be seen that the enzymatic activity of AAO was higher and led to the minimal FL intensity of MQDs/CoOOH nanoflakes/AA/AAO system at pH of 7.4 and reaction temperature of 37 °C. As shown in Fig. S5C, the FL intensity of MQDs/CoOOH nanoflakes/AA/AAO system constantly decreased with the increase of reaction time and kept unchangeable after 20 min, indicating the enzymatic reaction was completely. So pH of 7.4, temperature of 37 °C and reaction time of 20 min were selected as the optimal enzymatic reaction conditions for the subsequent experiments.

### 3.4. Determination of AAO

Fig. 4A showed the FL emission spectra of MQDs/CoOOH nanoflakes/AA system with various concentrations of AAO. It can be seen that the FL intensity of MQDs/CoOOH nanoflakes/AA system decreased gradually accompanied by a gradual increase in AAO concentrations from 0 to 70 mU $mL^{-1}$. Fig. 4B showed the relationship between the logarithm of relative FL intensity ($\Delta I/I_0$) and AAO concentrations. And lg ($\Delta I/I_0$) were linearly correlated with lg [AAO] in the AAO concentrations ranges of 2 mU $mL^{-1}$-10 mU $mL^{-1}$ and 10 mU $mL^{-1}$-40 mU $mL^{-1}$, respectively. The linear regression equations of lg ($\Delta I/I_0$) = 0.979 lg [AAO] – 1.449 ($R^2 = 0.998$) and lg ($\Delta I/I_0$) = 0.310 lg [AAO] - 0.798 ($R^2 = 0.999$) were obtained, respectively. And according to the first linear regression equation, the limit of detection (LOD) of the method for AAO detection was calculated to be 0.8 mU $mL^{-1}$ based on the 3σ rule. And the limit of quantification (LOQ) of 2.6 mU $mL^{-1}$ was obtained. The repeatability of the developed method for AAO assay was evaluated by measuring the relative standard deviation (RSD) of 10 mU $mL^{-1}$ AAO in five repeated measurements, and the RSD of 2.69% was obtained. And as shown in Table S1, the proposed FL method presented comparable analytical performance to that of previously reported sensing systems.

### 3.5. Selectivity and real sample measurements

To study the selectivity of the developed FL sensing method for AAO detection, the common metal ions (5 μg $mL^{-1}$ $K^+$, $Na^+$, $Cl^-$) and other biomolecules (0.25 μg $mL^{-1}$ urea, glucose, histidine, glycine, alanine, glucose oxidase, trypsin, hyaluronidase, pepsin, alkaline phosphatase) were applied for the selectivity measurements. As shown in Fig. 5, the FL signals of the MQDs/CoOOH nanoflakes/AA system toward the potentially interfering substances were almost the same as that of the blank sample with or without AAO, indicating there was a specific FL response to AAO and the proposed FL sensing method presented good selectivity toward AAO detection.

To further evaluate the potential application of the established system for AAO detection, several human serum samples were analyzed according to the standard addition method. As shown in Table 1, the acceptable recoveries from 96.8% to 102.7% with the RSDs ranging from 1.27% to 3.97% were obtained, which indicated the satisfactory applicability of this FL sensing method in real human serum samples.

## 4. Conclusion

In summary, a novel and sensitive FL strategy for AAO sensing was developed by taking advantage of the FL quenching of MQDs by CoOOH nanoflakes via FRET, the redox reaction between AA and CoOOH nanoflakes and the catalytic oxidation of AA by AAO. And the amount of AAO can be detected in the linear range of 2–10 mU $mL^{-1}$ and 10–40 mU $mL^{-1}$ with a low LOD of 0.8 mU $mL^{-1}$. The proposed sensing method presented good sensitivity, accuracy and selectivity for AAO detection. Moreover, this proposed FL method was successfully applied for the detection of AAO in real sample analysis.

## Credit author statement

This manuscript was not published or is not under consideration for

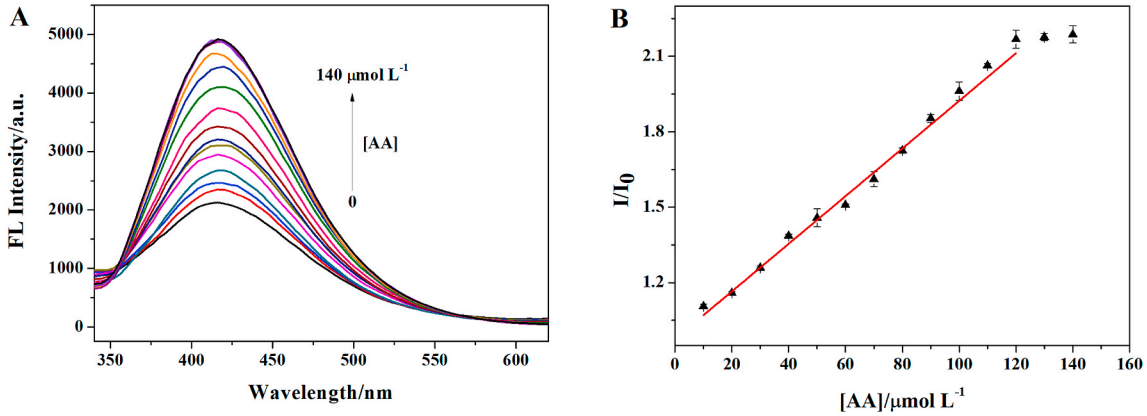


**Fig. 3.** (A) FL emission spectra of MQDs/CoOOH nanoflakes system at various concentrations of AA (0–140 μmol $L^{-1}$). (B) Plot of the relative FL intensity ($I/I_0$) as a function of AA concentrations (10, 20, 30, 40, 50, 60, 70, 80, 90, 100, 110, 120, 130, 140 μmol $L^{-1}$), where I and $I_0$ represent the FL intensity of the MQDs/CoOOH nanoflakes system in the presence and absence of AA, respectively.

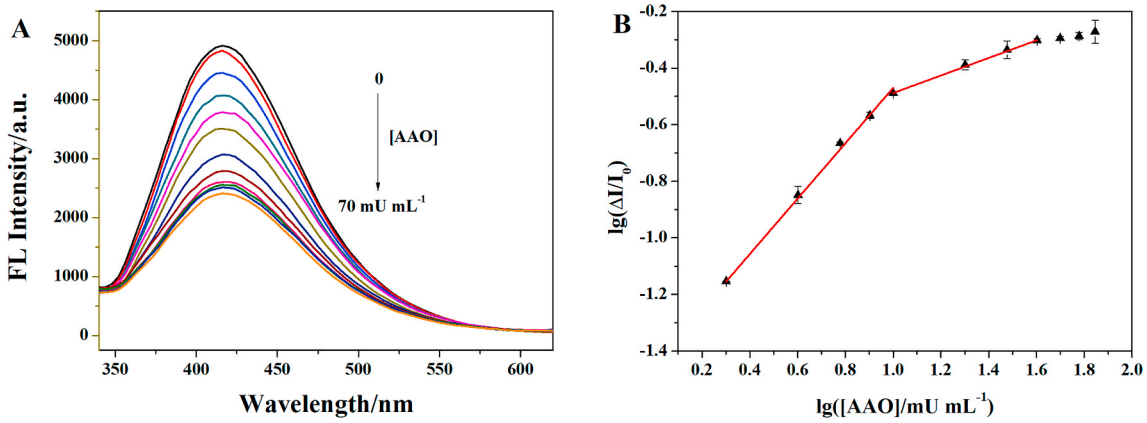


**Fig. 4.** (A) FL emission spectra of MQDs/CoOOH nanoflakes/AA system at various concentrations of AAO (0–70 mU $mL^{-1}$). (B) The relationship between the logarithm of relative FL intensity ($\Delta I/I_0$) and AAO concentrations (2, 4, 6, 8, 10, 20, 30, 40, 50, 60, 70 mU $mL^{-1}$), where $\Delta I = I_0 - I$; I and $I_0$ represent the FL intensity of the MQDs/CoOOH nanoflakes/AA system in the presence and absence of AAO, respectively.

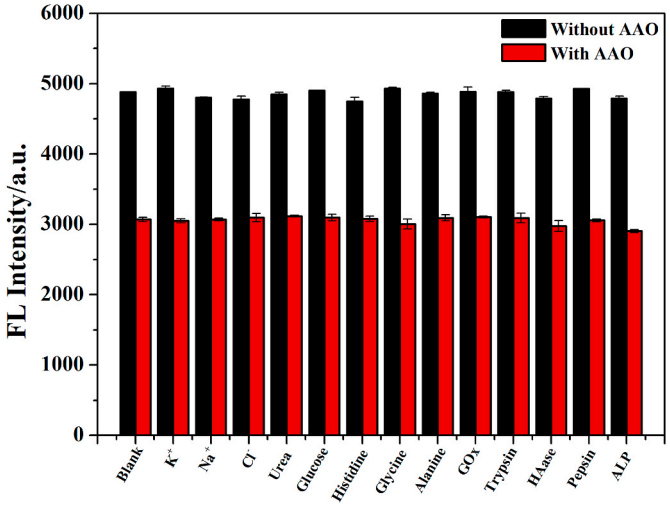


**Fig. 5.** The FL intensity of MQDs/CoOOH nanoflakes/AA system and the MQDs/CoOOH nanoflakes/AA/20 mU $mL^{-1}$ (0.05 μg $mL^{-1}$) AAO system with the potentially interfering substances: 5 μg $mL^{-1}$ $K^+$, $Na^+$, $Cl^-$ and 0.25 μg $mL^{-1}$ Urea, Glucose, Histidine, Glycine, Alanine, Glucose oxidase (GOx), Trypsin, Hyaluronidase (HAase), Pepsin, Alkaline phosphatase (ALP).

**Table 1**
Results of the recovery for AAO determination in serum samples.

| Sample | Added (mU $mL^{-1}$) | Founded (mU $mL^{-1}$) | Recovery (%) | RSD (%, n = 3) |
|---|---|---|---|---|
| 1 | 0 | – | – | 2.87 |
| 2 | 3.0 | 3.08 | 102.7 | 3.97 |
| 3 | 6.0 | 5.89 | 98.2 | 1.27 |
| 4 | 9.0 | 8.71 | 96.8 | 3.16 |

publication elsewhere. And I affirm that all authors have read and approved the submission of the revised manuscript.

## Declaration of competing interest

The authors declare that they have no known competing financial interests or personal relationships that could have appeared to influence the work reported in this paper.

## Acknowledgments

This work is supported by the National Natural Science Foundation of China (No. 21775052 and No. 21575048) and the Science and Technology Development project of Jilin province, China (No. 20180414013GH).

## Appendix A. Supplementary data

Supplementary data related to this article can be found at https://doi.org/10.1016/j.talanta.2020.121522.

## References

[1] G. Pereira, C. Monteiro, G. Albuquerque, M. Pereira, M. Cabrera, P. Cabral, G. Pereira, A. Fontes, B. Santos, (Bio)conjugation strategies applied to fluorescent semiconductor quantum dots, J. Braz. Chem. Soc. 30 (2019) 2536–2560.
[2] L. Su, X. Fan, T. Yin, H. Wang, Y. Li, F. Liu, J. Li, H. Zhang, H. Xie, Inorganic 2D luminescent materials: structure, luminescence modulation, and applications, Adv. Opt. Mater. 8 (2019) 1900978.
[3] A. Manikandan, Y.-Z. Chen, C.-C. Shen, C.-W. Sher, H.-C. Kuo, Y.-L. Chueh, A critical review on two-dimensional quantum dots (2D QDs): from synthesis toward applications in energy and optoelectronics, Prog. Quant. Electron. 68 (2019) 100226.
[4] T. Jamieson, R. Bakhshi, D. Petrova, R. Pocock, M. Imani, A.M. Seifalian, Biological applications of quantum dots, Biomaterials 28 (2007) 4717–4732.
[5] B.L. Li, M.I. Setyawati, H.L. Zou, J.X. Dong, H.Q. Luo, N.B. Li, D.T. Leong, Emerging 0D transition-metal dichalcogenides for sensors, biomedicine, and clean energy, Small 13 (2017) 1700527.
[6] Z. Sun, J. He, M. Yuan, L. Lin, Z. Zhang, Z. Kang, Q. Liao, H. Li, G. Sun, X. Yang, R. Long, Y. Zhang, Li+-clipping for edge S-vacancy MoS2 quantum dots as an efficient bifunctional electrocatalyst enabling discharge growth of amorphous Li2O2 film, Nanomater. Energy 65 (2019) 103996.
[7] C. Sweet, A. Pramanik, S. Jones, P.C. Ray, Two-photon fluorescent molybdenum disulfide dots for targeted prostate cancer imaging in the biological II window, ACS Omega 2 (2017) 1826–1835.
[8] S. Xu, D. Li, P. Wu, One-pot, facile, and versatile synthesis of monolayer MoS2/WS2Quantum dots as bioimaging probes and efficient electrocatalysts for hydrogen evolution reaction, Adv. Funct. Mater. 25 (2015) 1127–1136.
[9] S.-C. Chen, C.-Y. Lin, T.-L. Cheng, W.-L. Tseng, 6-Mercaptopurine-Induced fluorescence quenching of monolayer MoS2 nanodots: applications to glutathione sensing, cellular imaging, and glutathione-stimulated drug delivery, Adv. Funct. Mater. 27 (2017) 1702452.
[10] T. Wang, X. Hu, X. Zhang, H. Cao, Y. Huang, P. Feng, MoS2 QDs co-catalytic Fenton reaction for highly sensitive photoluminescence sensing of H2O2 and glucose, Anal. Methods 11 (2019) 415–420.
[11] H. Swaminathan, K. Balasubramanian, Förster resonance energy transfer between MoS2 quantum dots and polyaniline for turn-on bovine serum albumin sensing, Sensor. Actuator. B Chem. 264 (2018) 337–343.
[12] M.C. De Tullio, S. Ciraci, R. Liso, O. Arrigoni, Ascorbic acid oxidase is dynamically regulated by light and oxygen. A tool for oxygen management in plants? J. Plant Physiol. 164 (2007) 39–46.
[13] S.Y. Leong, I. Oey, D.J. Burritt, A novel strategy using pulsed electric fields to modify the thermostability of ascorbic acid oxidase in different carrot cultivars, Food Bioprocess Technol. 8 (2014) 811–823.

[14] V. Zelinová, Ľ. Halušková, I. Mistrík, L. Tamás, Abiotic stress–induced inhibition of root growth and ascorbic acid oxidase activity in barley root tip is associated with enhanced generation of hydrogen peroxide, Plant Soil 349 (2011) 281–289.
[15] Y. Zhang, H. Li, W. Shu, C. Zhang, W. Zhang, Z. Ye, Suppressed expression of ascorbate oxidase gene promotes ascorbic acid accumulation in tomato fruit, Plant Mol. Biol. Rep. 29 (2010) 638–645.
[16] M.C. De Tullio, R. Liso, O. Arrigoni, Ascorbic acid oxidase: an enzyme in search of a role, Biol. Plantarum 48 (2004) 161–166.
[17] V. Zelinová, Ľ. Halušková, I. Mistrík, L. Tamás, Abiotic stress–induced inhibition of root growth and ascorbic acid oxidase activity in barley root tip is associated with enhanced generation of hydrogen peroxide, Plant Soil 349 (2011) 281–289.
[18] J. Sekiya, K. Mizuno, O. Kimura, N. Shimose, Ascerbate oxidase in cucumber calli and enhancement of enzyme activity by copper sulfate, Soil Sci. Plant Nutr. 36 (1990) 43–51.
[19] M. Wang, M. Wang, G. Wang, X. Su, A fluorescence "off-on-off" sensing platform based on bimetallic gold/silver nanoclusters for ascorbate oxidase activity monitoring, Analyst 145 (2020) 1001–1007.
[20] X.Y. Han, Z.H. Chen, Q.X. Fan, K.N. Li, F.Y. Mu, Q. Luo, Z. Jin, G. Shi, M. Zhang, Manganese(II)-doped zinc/germanium oxide nanoparticles as a viable fluorescent probe for visual and time-resolved fluorometric determination of ascorbic acid and its oxidase, Microchim. Acta 186 (2019) 466.
[21] Y. Wang, Y. Yang, W. Liu, F. Ding, P. Zou, X. Wang, Q. Zhao, H. Rao, A carbon dot-based ratiometric fluorometric and colorimetric method for determination of ascorbic acid and of the activity of ascorbic acid oxidase, Microchim. Acta 186 (2019) 246.
[22] S. Liu, S. Pang, A dual-model strategy for fluorometric determination of ascorbic acid and of ascorbic acid oxidase activity by using DNA-templated gold-silver nanoclusters, Microchim. Acta 185 (2018) 426.
[23] J. Huang, J. Chen, T. Yao, J. He, S. Jiang, Z. Sun, Q. Liu, W. Cheng, F. Hu, Y. Jiang, Z. Pan, S. Wei, CoOOH nanosheets with high mass activity for water oxidation, Angew. Chem. Int. Ed. 54 (2015) 8722–8727.
[24] Z.-M. Li, X.-L. Zhong, S.-H. Wen, L. Zhang, R.-P. Liang, J.-D. Qiu, Colorimetric detection of methyltransferase activity based on the enhancement of CoOOH nanozyme activity by ssDNA, Sensor. Actuator. B Chem. 281 (2019) 1073–1079.
[25] S.H. Wen, X.L. Zhong, Y.D. Wu, R.P. Liang, L. Zhang, J.D. Qiu, Colorimetric assay conversion to highly sensitive electrochemical assay for bimodal detection of arsenate based on cobalt oxyhydroxide nanozyme via arsenate absorption, Anal. Chem. 91 (2019) 6487–6497.
[26] Y. Lv, C. Jiang, K. Hu, Y. Huang, Y. He, X. Shen, S. Zhao, In-situ growth of cobalt oxyhydroxide on graphitic-phase C3N4 nanosheets for fluorescence turn-on detection and imaging of ascorbic acid in living cells, Microchim. Acta 186 (2019) 360.
[27] J. Zhou, Y. Ling, N.B. Li, H.Q. Luo, Fluorometric and resonance Rayleigh scattering dual-mode bioprobe for determination of the activity of alkaline phosphatase based on the use of CoOOH nanoflakes and cobalt(II)-dependent DNAzyme-assisted amplification, Microchim. Acta 186 (2019) 437.
[28] L. Li, C. Wang, K. Liu, Y. Wang, K. Liu, Y. Lin, Hexagonal cobalt oxyhydroxide-carbon dots hybridized surface: high sensitive fluorescence turn-on probe for monitoring of ascorbic acid in rat brain following brain ischemia, Anal. Chem. 87 (2015) 3404–3411.
[29] H.M. Meng, X.B. Zhang, C. Yang, H. Kuai, G.J. Mao, L. Gong, W. Zhang, S. Feng, J. Chang, Efficient two-photon fluorescence nanoprobe for turn-on detection and imaging of ascorbic acid in living cells and tissues, Anal. Chem. 88 (2016) 6057–6063.
[30] W. Xu, J. Chen, S. Sun, Z. Tang, K. Jiang, L. Song, Y. Wang, C. Liu, H. Lin, Fluorescent and photoacoustic bifunctional probe for the detection of ascorbic acid in biological fluids, living cells and in vivo, Nanoscale 10 (2018) 17834–17841.
[31] S.G. Liu, D. Luo, L. Han, N.B. Li, H.Q. Luo, A hybrid material composed of guanine-rich single stranded DNA and cobalt(III) oxyhydroxide (CoOOH) nanosheets as a fluorescent probe for ascorbic acid via formation of a complex between G-quadruplex and thioflavin T, Microchim. Acta 186 (2019) 156.
[32] L.L. Feng, Y.X. Wu, D.L. Zhang, X.X. Hu, J. Zhang, P. Wang, Z.L. Song, X.B. Zhang, W. Tan, Near infrared graphene quantum dots-based two-photon nanoprobe for direct bioimaging of endogenous ascorbic acid in living cells, Anal. Chem. 89 (2017) 4077–4084.
[33] Y. Wang, Y. Ni, Molybdenum disulfide quantum dots as a photoluminescence sensing platform for 2,4,6-trinitrophenol detection, Anal. Chem. 86 (2014) 7463–7470.
[34] J. Liu, D. Tang, Z. Chen, X. Yan, Z. Zhong, L. Kang, J. Yao, Chemical redox modulated fluorescence of nitrogen-doped graphene quantum dots for probing the activity of alkaline phosphatase, Biosens. Bioelectron. 94 (2017) 271–277.
[35] X. Guo, Y. Wang, F. Wu, Y. Ni, S. Kokot, The use of tungsten disulfide dots as highly selective, fluorescent probes for analysis of nitrofurazone, Talanta 144 (2015) 1036–1043.
[36] X. Zhu, J. Xiang, J. Li, C. Feng, P. Liu, B. Xiang, Tunable photoluminescence of MoS2 quantum dots passivated by different functional groups, J. Colloid Interface Sci. 511 (2018) 209–214.
[37] H. Huang, C. Du, H. Shi, X. Feng, J. Li, Y. Tan, W. Song, Water-soluble monolayer molybdenum disulfide quantum dots with upconversion fluorescence, Part. Part. Syst. Char. 32 (2015) 72–79.
[38] H. Dong, S. Tang, Y. Hao, H. Yu, W. Dai, G. Zhao, Y. Cao, H. Lu, X. Zhang, H. Ju, Fluorescent MoS2 quantum dots: ultrasonic preparation, up-conversion and down-conversion bioimaging, and photodynamic therapy, ACS Appl. Mater. Interfaces 8 (2016) 3107–3114.
[39] H. Zhang, Z. Wang, X. Yang, Z.L. Li, L. Sun, J. Ma, H. Jiang, The determination of alpha-glucosidase activity through a nano fluorescent sensor of F-PDA-CoOOH, Anal. Chim. Acta 1080 (2019) 170–177.
[40] C. Chen, C. Midelet, S. Bhuckory, N. Hildebrandt, M.H.V. Werts, Nanosurface energy transfer from long-lifetime terbium donors to gold nanoparticles, J. Phys. Chem. C 122 (2018) 17566–17574.
[41] Q. Ma, X.G. Su, X.Y. Wang, Y. Wan, C.L. Wang, B. Yang, Q.H. Jin, Fluorescence resonance energy transfer in doubly-quantum dot labeled IgG system, Talanta 67 (2005) 1029–1034.